nature physics

SUPPLEMENTARY INFORMATION

DOI: 10.1038/NPHYS2272

Emergence of superlattice Dirac points in graphene on hexagonal boron nitride

Matthew Yankowitz,[1] Jiamin Xue,[1] Daniel Cormode,[1] Javier D. Sanchez-Yamagishi,[2] K. Watanabe,[3] T. Taniguchi,[3] Pablo Jarillo-Herrero,[2] Philippe Jacquod,[1,4] and Brian J. LeRoy[1,*]

[1]*Physics Department, University of Arizona, 1118 E 4th Street, Tucson, AZ 85721, USA*

[2]*Department of Physics, Massachusetts Institute of Technology, Cambridge, MA 02138, USA*

[3]*Advanced Materials Laboratory, National Institute for Materials Science, 1-1 Namiki, Tsukuba 305-0044, Japan*

[4]*Département de Physique Théorique, Université de Genève CH-1211 Genève, Switzerland*

*Electronic address: leroy@physics.arizona.edu

I. DERIVATION OF MOIRÉ WAVELENGTH AND ANGLE

The expression for the Moiré wavelength as a function of relative rotation angle ϕ between the graphene and hBN lattices can be found using the reciprocal lattices. Consider one of the reciprocal lattice vectors of graphene denoted $\mathbf{g}$. This vector can be chosen to be along the x axis and written as

$$\mathbf{g} = \frac{2\pi}{a}(1, 0), \tag{1}$$

where a is the graphene lattice constant. The corresponding reciprocal lattice vector for hBn is shorter given the lattice mismatch δ between hBN and graphene. The relative rotation angle ϕ between the two lattices gives a reciprocal lattice vector for hBN of

$$\mathbf{b} = \frac{2\pi}{(1+\delta)a}(\cos\phi, \sin\phi). \tag{2}$$

Letting $\mathbf{k}$ be the vector which connects the hBN reciprocal lattice vector to the graphene reciprocal lattice vector, we have that

$$\mathbf{k} = \mathbf{g} - \mathbf{b} = \frac{2\pi}{a}(1 - \frac{\cos\phi}{1+\delta}, -\frac{\sin\phi}{1+\delta}). \tag{3}$$

Then the wavelength of the Moiré pattern is given by $\lambda = \frac{2\pi}{|\mathbf{k}|}$. Since

$$|\mathbf{k}| = \frac{2\pi}{a}\sqrt{\left(1 - \frac{\cos\phi}{1+\delta}\right)^2 + \left(\frac{\sin\phi}{1+\delta}\right)^2} \tag{4}$$

a bit of algebra gives

$$\lambda = \frac{(1+\delta)a}{\sqrt{2(1+\delta)(1-\cos\phi) + \delta^2}} \tag{5}$$

which is the expression given in Eq. (1) in the main text.

The relative rotation angle θ of the Moiré pattern with respect to the graphene lattice is found by determining the angle of the reciprocal lattice vector $\mathbf{k}$ with respect to the graphene reciprocal lattice vector. Since, we chose the x-axis for the graphene reciprocal lattice vector, the angle of the Moiré pattern is given by

$$\tan\theta = \frac{-k_y}{k_x} = \frac{\frac{\sin\phi}{1+\delta}}{1 - \frac{\cos\phi}{1+\delta}}. \tag{6}$$

Simplifying this equation gives the result for Eq. (2) in the main text,

$$\tan\theta = \frac{\sin\phi}{(1+\delta) - \cos\phi}. \tag{7}$$

II. LOW ENERGY PERTURBATION THEORY

Scattering at the Brillouin zone boundaries due to the periodic potential does not open a gap for chiral massless Dirac fermions as long as sublattice symmetry is preserved. This can be seen by performing a unitary transformation $\hat{H} \to \hat{H}' = U_1^\dagger \hat{H} U_1$ on the Hamiltonian in the main text,

$$\hat{H} = \hbar v_{\rm F} \mathbf{k} \cdot \vec{\sigma} + V \sum_\alpha \cos(\mathbf{G}_\alpha \mathbf{x})\, \mathcal{I}\,, \tag{8}$$

with $U_1 = \exp[i\vec{\Lambda}(\mathbf{r}) \cdot \vec{\sigma}]$. When $V/\hbar v_{\rm F}|\mathbf{G}| < 1$ the linear part of the potential can be gauged out of the Hamiltonian for $\hbar v_{\rm F} \nabla \cdot \vec{\Lambda} = -\hat{V}$. For $V/\hbar v_{\rm F}|G| > 1$, the gauge transformation can no longer remove the linear part of the potential, and the potential creates new Dirac points at zero energy but still does not open a gap. [1–5].

The magnitude of the dips in the local density of states (LDOS) is determined by the strength and the wavelength of the Moiré periodic potential. We see this perturbatively by projecting the Hamiltonian of Eq. (8) onto the pairs of eigenstates

$$\psi_{s,\mathbf{k}} = (1, s\exp[i\theta_{\mathbf{k}}])^T \exp[i\mathbf{kr}]/\sqrt{2\Omega}$$

of $\hat{H}_0 = \hbar v_{\rm F} \mathbf{k} \cdot \vec{\sigma}$, with the lattice area Ω, the band index $s = 1$ for the conduction, $s = -1$ for the valence band, and the angle $\theta_{\mathbf{k}} = \arctan(k_y/k_x)$. The resulting 2×2 Hamiltonian reads

$$\hat{H}_{\rm red} = \begin{pmatrix} s\hbar v_{\rm F} k & V_{k,k'} \\ (V_{k,k'})^* & s\hbar v_{\rm F} k' \end{pmatrix}\,, \tag{9}$$

with $V_{k,k'} = (V/4)(1 + \exp[i(\theta_{\mathbf{k}'} - \theta_{\mathbf{k}})]) \sum_\alpha (\delta_{\mathbf{k},\mathbf{G}_\alpha+\mathbf{k}'} + \delta_{\mathbf{k},-\mathbf{G}_\alpha+\mathbf{k}'})$. We focus on momenta $\mathbf{k} = \mathbf{G}_\alpha/2 + \delta\mathbf{k}$, $\mathbf{k}' = -\mathbf{G}_\alpha/2 + \delta\mathbf{k}$. For this choice of pairs of eigenstates, it is straightforward to see that the eigenvalues of $\hat{H}_{\rm red}$ are $E_\pm = (\varepsilon_+ + \varepsilon_-)/2 \pm \sqrt{(\varepsilon_+ - \varepsilon_-)^2 + (V\delta k_\perp/G)^2}/2 + \mathcal{O}(\delta k^2/G^2)$, with $\varepsilon_\pm = \hbar v_{\rm F}|\mathbf{G}_\alpha/2 \pm \delta\mathbf{k}|$, and the component $\delta k_\perp$ of $\delta\mathbf{k}$ that is perpendicular to $\mathbf{G}_\alpha$. For $|\delta\mathbf{k}| \ll G$, this gives an anisotropic linear dispersion with a new Fermi velocity $v'_{\rm F}(\delta\theta) = \sqrt{(v_{\rm F}\cos\delta\theta)^2 + (V\sin\delta\theta/2\hbar G)^2}$ with the angle $\delta\theta$ between $\delta\mathbf{k}$ and $\mathbf{G}_\alpha$. The Fermi velocity at the new Dirac point further reduces to the result of Ref. [2] for the simpler case of a one-dimensional potential (with a single $\mathbf{G}_\alpha$). This perturbative result is consistent with the numerical and experimental facts reported here that (i) no gap is opened, neither in the numerically obtained $\rho(E, \mathbf{r})$, nor in the experimentally obtained STM dI/dV, (ii) a reduction of (dip in) the density of states is observed at an energy corresponding to $\hbar v_{\rm F} G/2$,

and (iii) both the spectroscopic Moiré pattern and the dips tend to disappear for periodic potentials with shorter wavelength (hence larger G), when the relative rotation between the hBN substrate and the graphene layer is larger. The reduction of the density of states occurs around three points determined by the three reciprocal lattice vectors. At this level, there is no s-dependence of the strength of the dip, the latter is the same for $s = 1$ ($E > 0$) as for $s = -1$ ($E < 0$). An s-dependence emerges once off-diagonal terms $\sim V'\sigma^{x,y}$ are included in the Hamiltonian of Eq. (8).

III. BILAYER LATTICE HAMILTONIAN FOR GRAPHENE ON HEXAGONAL BORON NITRIDE

We consider a lattice Hamiltonian for a graphene monolayer on a single layer of hBN. For each layer, the Hamiltonian reads

$$\mathcal{H}_\alpha = \sum_i \left[\epsilon_A(\alpha) a_i^\dagger(\alpha) a_i(\alpha) + \epsilon_B(\alpha) b_i^\dagger(\alpha) b_i(\alpha)\right] - t_\alpha \sum_{\langle i,j\rangle} (a_i^\dagger(\alpha) b_j(\alpha) + h.c.)\,, \qquad (10)$$

where $a_i^\dagger(\alpha)$ [$a(\alpha)$] and $b_i^\dagger(\alpha)$ [$b(\alpha)$] are creation [destruction] operators on sublattice A and B, respectively, of the graphene ($\alpha = 1$) or hBN ($\alpha = 2$) honeycomb lattice, and $\langle i, j\rangle$ indicates that the sum runs only over nearest neighbors. On the hBN lattice, we choose the Boron atoms to be on the A sublattice and the Nitrogen atoms to be on the B sublattice. The on-site energies are $\epsilon_A(1) = \epsilon_B(1) = 0$, $\epsilon_A(2) = 3.34$ eV and $\epsilon_B(2) = -1.4$ eV, and the hopping integrals are $t_1 = 3.16$ eV and $t_2 = 2.79$ eV [6] (the precise value of the latter is of little importance).

We restrict the interlayer hopping potential to nearest-neighbor and next-nearest-neighbor hopping. The interlayer hopping is given by

$$t'_{ij}(m,n) \;=\; \gamma_\perp \exp[-|\mathbf{r}_i(m) - \mathbf{r}_j(n)|/\xi]\, f_{ij}\,, \qquad (11)$$

with a characteristic function $f_{ij} = 1$ if site i of sublattice m on the graphene (hBN) sheet is nearest or next-nearest neighbor to site j of sublattice n on the hBN (graphene) sheet, and $f_{ij} = 0$ otherwise. The parameters $\gamma_\perp = 0.39$ eV and $\xi = 0.032$ nm are calibrated to fit the interlayer couplings in bilayer graphene[7]. The two lattices are rotated with respect to one another by the angle ϕ, and for each site we determine its nearest and next nearest neighbor site on the other sheet, numerically evaluate the distance between the sites and

finally the corresponding interlayer hopping. While $\gamma_\perp$ should in principle depend on the sublattice index in the hBN layer, we neglect this dependence here. The interlayer coupling Hamiltonian is then given by

$$\mathcal{H}_\perp = -\sum_{ij}\Big[t'_{ij}(A,A)[a_i^\dagger(1)a_j(2)+h.c.]+t'_{ij}(A,B)[a_i^\dagger(1)b_j(2)+h.c.] \\ +t'_{ij}(B,A)[b_i^\dagger(1)a_j(2)+h.c.]+t'_{ij}(B,B)[b_i^\dagger(1)b_j(2)+h.c.]\Big]\ . \qquad (12)$$

Second-order perturbation theory maps $\mathcal{H}_\perp$ onto a periodic potential of hexagonal symmetry, similar to the one in Eq. (8), with a modulation amplitude $V \simeq 0.06$ eV which we determined numerically via second order perturbation theory in the interlayer hopping. This energy is smaller than $\hbar v_{\rm F}|\mathbf{G}|/2$ with the Moiré superlattice vector $\mathbf{G}$, regardless of the rotation angle between graphene and hBN sheets.

The total Hamiltonian reads $\mathcal{H}_1+\mathcal{H}_2+\mathcal{H}_\perp$. We evaluate the LDOS $\rho(\mathbf{r}_i,E)$ on the graphene sheet using the Lanczos method, which allows to reach linear system sizes of $L=1000$ or more sites [8]. The obtained $\rho(\mathbf{r},E)$ depends on a smearing parameter ζ which, as long as the density of states of the STM tip and the tunneling rate from the tip to the sample do not depend on energy can be related to the strength of the tip-graphene coupling. Figure S1(a) illustrates how reducing this coupling allows finer and finer structures in the LDOS to be explored. For this particular rotation of $\phi = 0.3^o$, corresponding to a Moiré pattern with $\lambda = 13.4$ nm, and the set of parameters we just discussed, we see that the LDOS vanishes more or less linearly close to $E - E_{\rm D} = -\hbar v_{\rm F}|\mathbf{G}|/2$. Our numerical data suggest a complete, linear vanishing of the LDOS there. The linear vanishing of the LDOS, gives an estimate for the Fermi velocity close to the three new superlattice Dirac points. We estimate that the new velocity for the holes is $(0.73\pm0.08)v_{\rm F}$. The new velocity for electrons is smaller because of the increased slope and we estimate it to be $(0.53\pm0.05)v_{\rm F}$. The new reduced Fermi velocities are in reasonable agreement with our experimentally determined values.

A significant energy asymmetry emerges in that the expected dip in the density of states is stronger in the valence $E<0$ than in the conduction $E>0$ band. This asymmetry arises because of (i) the asymmetry in the on-site energies in the hBN layer, which effectively induces a second order potential that is stronger for negative than for positive energies and (ii) next-nearest neighbor interlayer hopping, which effectively induces a local periodic modulation of t_1. This is illustrated in Fig. S1(b).

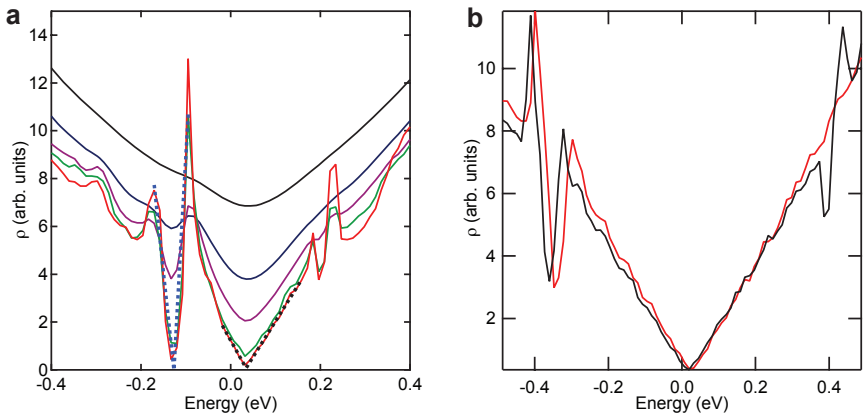

Figure S1: Calculated density of states as a function of coupling. (a) LDOS for a 1000×1000 graphene lattice on a hBN sheet, with relative rotation $\phi = 0.3^o$. The smearing parameter of the Lanczos algorithm is $\zeta = 0.09$ (black curve), 0.04 (red), 0.018 (green), 0.008 (blue) and 0.0036 (violet). The dashed lines give linear fits close to the Dirac and superlattice Dirac points. (b) LDOS for a 1000×1000 graphene lattice on a hBN sheet, with relative rotation $\phi = 2.0^o$, for $\zeta = 0.0036$. The black curve has nearest-neighbor interlayer coupling, the red curve has nearest and next nearest neighbor interlayer hopping.

IV. BAND STRUCTURE CALCULATION

We perform a band structure calculation to show that a weak interlayer coupling does not open a gap, but instead creates new Dirac points at energies determined by the relative rotation between the layers. We project the low-energy Hamiltonian of Eq. (8) on fourteen states with $\mathbf{k}$ and $\mathbf{k} \pm \mathbf{G}_\alpha$, where the periodic potential's reciprocal lattice vectors $\mathbf{G}_\alpha$ ($\alpha = 1, 2, 3$) are determined by the relative rotation of the two lattices as described earlier. In Fig. S2(a), we show the dispersions of the valence bands with energies closest to the original Dirac point ($E = 0$) for a rotation angle $\phi = 0.285$ (corresponding to a Moiré wavelength of $\lambda = 13.4$ nm). This confirms that the weak interlayer coupling opens new Dirac points with anisotropic dispersion. Fig. S2(b) and (c) show contour plots of the bands indicating the locations of the new superlattice Dirac points. Similar results can be seen in the conduction bands. We note that for the new superlattice Dirac point close to $\mathbf{G}_\alpha/2$, the velocity in the direction perpendicular to $\mathbf{G}_\alpha$ is smaller for larger relative lattice rotation and larger $|\mathbf{G}|$, as predicted by our perturbative treatment in Section II.

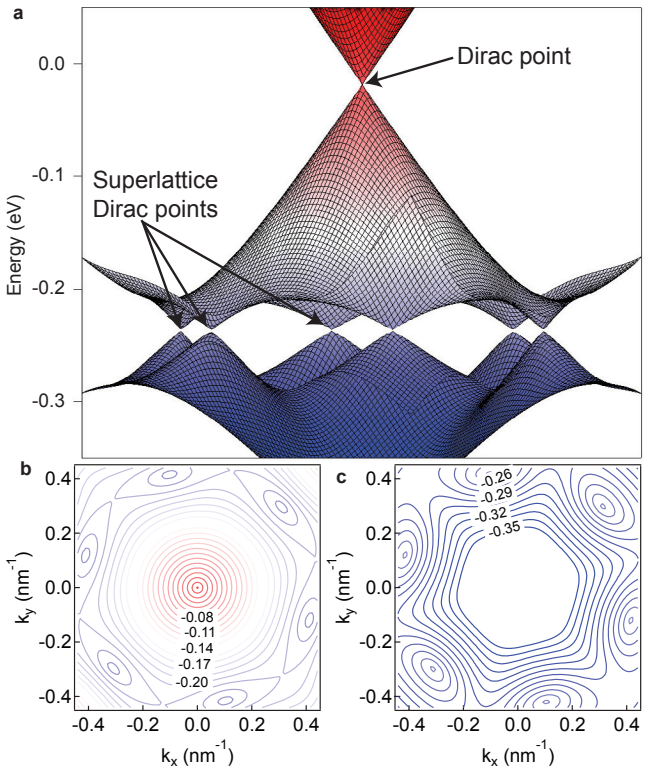

Figure S2: Dispersion relation for graphene with a weak periodic potential. (a) Energy of the valence bands as a function of wavevector showing the original Dirac point and the emergence of new superlattice Dirac points. (b) Contour plot of the upper most valence band showing the original Dirac point at the center and the new superlattice Dirac points near the edges. (c) Contour plot of the next highest valence band showing the locations of the superlattice Dirac points.

V. FITTING ANISOTROPIC FERMI VELOCITIES

Our low energy perturbation theory results as well as previous theoretical calculations for graphene subjected to a periodic potential have predicted an anisotropic Dirac cone at an energy of $\hbar v_{\mathrm{F}}|\mathbf{G}|/2$ [2]. This leads to different Fermi velocities as a function of angle with respect to the periodic potential. Our measurements are only able to obtain a single value for the Fermi velocity because we are only sensitive to the density of states. The density of states gives the area of the constant energy contours but not their precise shape. In the fitting of Fig. 3(b) near the energy of the superlattice Dirac cone, we have assumed an elliptical constant energy contour. For a symmetric Dirac cone, the constant energy contour is a circle. Therefore the number of states is given by $N = g_v g_s \pi k^2/(2\pi)^2$, where $g_s = 2$

is the spin degeneracy and $g_v = 6$ is the valley degeneracy. Since the dispersion relation is given by $E(k) = \hbar v_{\rm F} k$, we can write $E = \hbar v_{\rm F}\sqrt{4\pi N/g_v g_s}$. Then the number of electrons induced by the gate electrode is proportional to its voltage giving Eq. (3) of the main text,

$$E_{\rm D} = \hbar v_{\rm F}\sqrt{2\pi\alpha(V_g - V_o)/g_v}$$

If the Dirac cone is asymmetric, the constant energy contour is an ellipse, with different Fermi velocities along different momentum directions. Using our perturbation theory results, we find that the Fermi velocity along the direction of the superlattice potential is unmodified. Therefore, in this direction $E(k_x) = \hbar v_{\rm F}^0 k_x$. In the direction perpendicular to the potential, the Fermi velocity is reduced and $E(k_y) = \hbar v_{\rm F}^* k_y$ with $v_{\rm F}^* = V/2\hbar G$. With our perturbation theory result we obtain that the expected shift of the Dirac point with gate voltage is

$$E_D = \hbar\sqrt{v_{\rm F}^0 v_{\rm F}^* 2\pi\alpha(V_g - V_o)/g_v}$$

where $v_{\rm F}^0$ is the unperturbed Fermi velocity and $v_{\rm F}^*$ is the reduced Fermi velocity. This is the expression that was used to obtain the fits of Fig. 3(b).

VI. TRANSPORT MEASUREMENT

We have also performed electrical transport measurements on the graphene device shown in Fig. 3. The conductivity as a function of gate voltage is shown in Fig. S3. The gate voltage is plotted as the offset from the gate voltage at the Dirac point. We observe two locations of decreased conductivity which are located at approximately ±40 V from the Dirac point. This is the same separation in gate voltage as observed in the spectroscopy measurements, where the main Dirac point was separated from the superlattice Dirac point by 40 V. Therefore, we conclude that the dips in conductivity are due to the presence of the superlattice Dirac point. This gives further indirect evidence of the superlattice Dirac point. We also see a second dip in the conductivity near -50 V. Our STM topography measurements showed a region of the device with a second Moiré pattern of about 10 nm. The superlattice Dirac point due to this Moiré occurs at a higher energy and hence a larger gate voltage.

[1] Park, C.-H., Yang, L., Son, Y.-W., Cohen, M. L., and Louie, S. G. Anisotropic behaviours of massless Dirac fermions in graphene under periodic potentials. *Nature Phys.* **4**, 213-217 (2008);

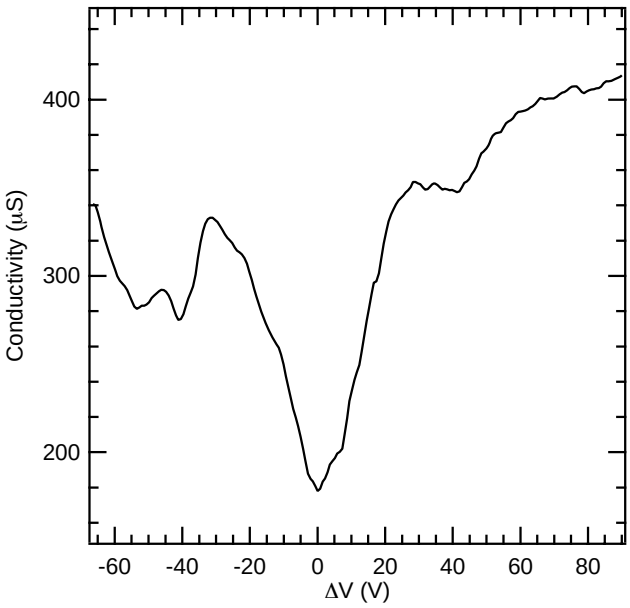

Figure S3: Conductivity as a function of gate voltage for the graphene device with a 13.4 nm Moiré pattern.

[2] Park, C.-H., Yang, L., Son, Y.-W., Cohen, M. L., and Louie, S. G. New generation of massless Dirac fermions in graphene under external periodic potentials. *Phys. Rev. Lett.* **101**, 126804 (2008).

[3] Park, C.-H., Son, Y.-W., Yang, L., Cohen, M. L., and Louie, S. G. Landau levels and quantum Hall effect in graphene superlattices. *Phys. Rev. Lett.* **103**, 046808 (2009).

[4] Brey, L. and Fertig, H. A. Emerging zero modes for graphene in a periodic potential. *Phys. Rev. Lett.* **103**, 046809 (2009).

[5] Sun, J., Fertig, H. A., and Brey, L. Effective magnetic fields in graphene superlattices. *Phys. Rev. Lett.* **105**, 156801 (2010).

[6] Xue, J. *et al.* Scanning tunnelling microscopy and spectroscopy of ultra-flat graphene on hexagonal boron nitride. *Nature Mater.* **10**, 282-285 (2011).

[7] Zhang, L. M. *et al.* Determination of the electronic structure of bilayer graphene from infrared spectroscopy. *Phys. Rev. B* **78**, 235408 (2008).

[8] Dagotto, E. Correlated electrons in high-temperature superconductors. *Rev. Mod. Phys.* **66**, 763-840 (1994).